Propagation-Aware Link Budget and Availability Analysis of a 15 GHz TETRA Radio Relay Link in Mountainous and Tunnel Environments

Ana TATOVIC, Marina MILOSEVIC, Djordje DAMNJANOVIC

Dept. of Electrical Engineering, University of Kragujevac, Svetog Save 65, 32000 Cacak, Serbia

ana.tatovic@ftn.kg.ac.rs, marina.milosevic@ftn.kg.ac.rs, djordje.damnjanovic@ftn.kg.ac.rs

Submitted May 28, 2026 / Accepted July 12, 2026 / Online first July 31, 2026

Abstract. *Reliable design of radio relay links in complex propagation environments remains a significant challenge for mission-critical communication systems. This paper presents a propagation-aware link budget methodology that integrates terrain morphology, Fresnel zone clearance, atmospheric attenuation (including gaseous absorption and precipitation), and multipath propagation into a unified analytical framework in accordance with ITU-R recommendations. The main contribution lies in the systematic integration of multiple propagation mechanisms into a unified procedure for link availability estimation and propagation-aware radio-relay link assessment. A representative 15 GHz radio relay link between the Laz tunnel and the Ovcar site, designed for a capacity of 100 Mb/s within a TETRA system, is used as a case study for verification. Analytical calculations of received signal power, fade margin, and link availability are supported by simulation-based verification using Radio Mobile. Good agreement between analytical and simulation-based predictions was obtained, with a received signal level difference below 2 dB. Multipath propagation is identified as the dominant degradation mechanism, while rain attenuation has a secondary impact. The achieved link availability exceeds 99.99%, demonstrates practical applicability for the considered case study.*

Keywords

Radio relay link design, propagation-aware modeling, link budget analysis, multipath fading, TETRA communication systems

1. Introduction

The rapid expansion of modern transportation and critical infrastructure systems imposes increasingly stringent requirements on wireless communication network design [1], particularly in complex environments such as tunnels and mountainous regions. In such scenarios, ensuring continuous, reliable, and secure communication is essential for traffic safety, operational coordination, and emergency response. These requirements are especially important in mission-critical systems, where even short communication interruptions may lead to significant operational risks [2], [3].

TETRA (Terrestrial Trunked Radio) systems are widely deployed in such applications due to their high reliability, low latency, and support for prioritized group communication. However, achieving stable radio coverage in environments characterized by obstructed visibility and irregular terrain remains a significant challenge [4]. Under such conditions, signal propagation deviates from ideal free-space assumptions and becomes strongly influenced by terrain morphology, atmospheric conditions, and multipath propagation mechanisms, resulting in additional attenuation and signal fluctuations. Tunnel environments further exacerbate these effects due to confined geometry and pronounced multipath components [4]. Recent studies in TETRA systems have confirmed that signal propagation in such environments strongly depends on geometry, surface properties, and environmental conditions, significantly affecting overall link performance.

Accurate modeling of radio wave propagation is therefore essential for reliable link design and performance prediction. Classical approaches to radio system design provide a solid theoretical foundation, but often rely on simplified assumptions that do not fully capture the complexity of real propagation environments. Recent research indicates that propagation modeling remains an open challenge, particularly in complex environments where multiple mechanisms interact simultaneously, requiring more advanced and integrated approaches. Furthermore, modern studies emphasize that accurate representation of the propagation environment plays a crucial role in reliable link quality prediction in the millimeter-wave band [5].

Several recent works have addressed specific aspects of radio relay system design. Reference [6] focused on improving operational reliability through IT-based monitoring and control strategies, while [7] investigated

DOI: 10.13164/re.2026.0375

TETRA system design with emphasis on reliability indicators. An optimized planning tool for microwave links based on simulation-driven approaches is proposed in [8], while references [9] and [10] analyzed rain attenuation effects using advanced prediction models. In addition, recent work has proposed KPI-driven microwave link planning methodologies integrating line-of-sight analysis, link budget evaluation, and availability assessment for reliable backhaul deployment in challenging environments [11], while reference [12] compared relay techniques for long-distance transmission, and [13] extended relay concepts toward beyond-5G systems. Compared to previous studies addressing individual aspects of radio-relay system design, this work combines analytical modeling, simulation-based verification, and a real-case radio-relay link within a unified assessment framework. The presented case study demonstrates the practical applicability of the proposed workflow for the considered propagation conditions and may provide a basis for future investigations in similar environments.

At higher frequencies, propagation losses and sensitivity to environmental conditions become more pronounced, further emphasizing the need for accurate propagation-aware modeling [14]. Experimental studies conducted in realistic environments confirm that complex terrain and environmental conditions introduce significant deviations from ideal propagation models, directly affecting system performance and link reliability, as demonstrated in long-range communication systems such as LoRa [15]. Similar observations regarding the importance of accurate terrain representation in propagation prediction were reported in [16], where the influence of terrain sampling density on propagation model accuracy was analyzed for a 5G NR-V2X scenario. Although focused on a different application and frequency band, the results confirm that terrain morphology and propagation modeling accuracy have a significant impact on reliable link performance prediction. Therefore, a more comprehensive and physically grounded approach is required for accurate radio relay link design in such environments.

To address these challenges, radio relay systems are commonly employed as an efficient and cost-effective solution for extending coverage in areas with limited or obstructed line-of-sight (LoS). Compared to conventional base station deployments, relay-based architectures improve signal availability and overall system robustness. Although alternative backhaul solutions, such as optical fiber and public cellular networks, exist, they often fail to meet the required levels of availability and economic feasibility in challenging propagation conditions. Properly designed radio relay links, supported by accurate propagation modeling, provide high autonomy and stable performance.

The selected 15 GHz frequency band was adopted in accordance with the technical requirements of a TETRA communication network deployed for mission-critical services. The considered radio-relay link serves as a redundant transmission path for TETRA base stations located along a transportation corridor and provides connectivity between two geographically separated sites. The selected frequency range is widely used for fixed point-to-point microwave systems due to its favorable compromise between transmission capacity, antenna dimensions, and propagation performance over medium-distance links.

The frequency arrangement adopted in this study follows reference [18] which specifies channel arrangements for fixed wireless systems operating in the 14.4–15.35 GHz band. The selected duplex channel bandwidth of 28 MHz is consistent with practical radio-relay deployments and supports the required transmission capacity of 100 Mb/s.

From the regulatory perspective, the selected frequency band is consistent with the ITU-R [38], the ECC frequency allocation recommendations [37], and the national frequency allocation framework administered by the regulatory authority [36]. In practical radio-relay systems, channel assignment, licensing conditions, interference coordination, and frequency availability represent important design constraints. In the considered system, channel allocation is performed according to the applicable national regulations, while alternative channels may be selected in the event of co-channel or adjacent-channel interference.

Propagation characteristics at approximately 15 GHz are strongly influenced by rainfall attenuation, atmospheric gaseous absorption, multipath fading, and terrain-related effects. The present analysis explicitly considers these propagation mechanisms through the application of the corresponding ITU-R recommendations, allowing their combined influence on fade margin, availability, and link performance to be assessed. Consequently, the selected frequency band represents an appropriate case for demonstrating the practical application of propagation-aware radio-relay link assessment [9, 10, 14, 25, 27, 29, 31].

Compared to the authors' previous work [17], which focused on preliminary link design aspects, this paper extends the analysis by presenting a complete link budget calculation, together with availability analysis in accordance with ITU-R recommendations and comparison with simulation results using Radio Mobile, thereby providing a complete and practically applicable methodology for radio relay link design. Radio Mobile is a radio planning and propagation simulation tool based on digital terrain elevation data and the Longley–Rice propagation model. It enables terrain-profile extraction and prediction of key propagation characteristics for terrestrial radio links. It was employed to assess the consistency of the analytical predictions and to provide additional confirmation of the obtained propagation and link-budget results.

In contrast to existing approaches, this paper proposes an integrated propagation-aware framework for radio relay link design, which simultaneously accounts for terrain morphology, Fresnel zone clearance, atmospheric attenuation, rain effects, and multipath fading in accordance with ITU-R recommendations [18–31]. The proposed methodology combines analytical modeling with independent simulation results, enabling practical applicability and consistency assessment.

The proposed approach should not be interpreted as a new propagation model or a replacement for established ITU-R prediction methods. Its contribution lies in the structured integration of terrain analysis, atmospheric effects, fading prediction, availability assessment, and simulation-based verification within a unified radio-relay link assessment procedure.

The main contributions of this work can be summarized as follows:

- Development of a structured propagation-aware assessment workflow integrating terrain morphology, Fresnel-zone clearance, atmospheric attenuation, rain effects, multipath fading, and availability estimation within a unified link design procedure,
- Evaluation of link availability in accordance with ITU-R recommendations,
- Application of the proposed methodology to a representative 15 GHz TETRA radio relay link in a complex environment, between the Laz tunnel and the Ovcar site.
- Combined analytical and simulation-based assessment.

This paper is organized as follows: Section 2 presents the proposed propagation-aware radio relay link design methodology. Section 3 describes the outage probability analysis based on ITU-R recommendations, while Section 4 presents the radio relay link availability analysis. Section 5 provides the link budget results and discussion. Finally, Section 6 concludes the paper and outlines directions for future work.

2. Propagation-Aware Radio Relay Link Design Methodology

This section presents the proposed propagation-aware assessment procedure for radio relay link design. The approach is based on the integration of standard propagation models defined in ITU-R recommendations and established propagation theory. All equations adopted from the literature are explicitly referenced. The main contribution of this work is the integration of multiple propagation mechanisms, availability assessment procedures, and simulation-assisted evaluation into a unified propagation-aware assessment framework, rather than the development of new analytical expressions. The proposed approach enables practical radio-relay link performance evaluation under complex propagation conditions.

The selected operating frequency represents a practical microwave band widely used for fixed-service radio-relay applications. It provides a suitable compromise between available channel bandwidth, achievable transmission capacity, antenna dimensions, and propagation reliability for short- and medium-range microwave links. Compared with lower microwave frequency bands, it enables higher transmission capacities while maintaining relatively compact antenna dimensions and adequate link availability when appropriate fade margins are applied. These characteristics make this frequency range particularly suitable for mission-critical communication systems, where both high reliability and efficient spectrum utilization are required.

At the same time, propagation in this band becomes increasingly sensitive to atmospheric and environmental effects compared with lower microwave frequencies. Rain attenuation, gaseous absorption, and multipath fading therefore play a more significant role in determining link availability and fade-margin requirements. Consequently, accurate propagation-aware modeling becomes essential for reliable system design.

From a regulatory perspective, this frequency range belongs to bands allocated for fixed-service microwave applications and is governed by international, European, and national frequency-management frameworks. Its utilization is harmonized through relevant ITU and ECC/CEPT recommendations [37], [38], while national implementation is regulated through the Serbian National Frequency Allocation Plan administered by RATEL [36]. These frameworks define channel arrangements, spectrum usage conditions, and interference-management requirements that are essential for practical radio-relay system deployment.

In this study, the link design is based on key system parameters, including operating frequency, channel bandwidth, modulation scheme, polarization, and antenna characteristics and verified through simulation-based analysis. Particular emphasis is placed on propagation-related constraints, which play a dominant role in determining link performance in complex environments.

Efficient frequency planning must comply with regulatory frameworks [18], ensuring minimal interference and optimal spectrum utilization. Additionally, modern systems support hybrid traffic (Ethernet and TDM), adaptive modulation, and advanced network management functionalities.

Accurate link design requires detailed modeling of propagation conditions. Unlike simplified free-space approaches, real environments introduce additional losses due to terrain morphology, atmospheric effects, and multipath propagation. Multipath propagation [25], caused by reflection and scattering mechanisms, represents a key impairment in complex environments such as mountainous regions and tunnel surroundings, and must therefore be incorporated into the link budget analysis.

2.1 Path Profile Analysis

The first step in the design process is terrain profiling, based on digital elevation data, which enables verification of line-of-sight (LoS) conditions and identification of potential obstacles along the path. Environmental parameters such as temperature, atmospheric pressure, humidity, and rainfall significantly influence signal attenuation, particularly at higher frequencies. These effects are modeled using established ITU-R recommendations. The proposed design methodology is applied to a 15 GHz radio relay link between the Laz tunnel (Station A) and the Ovcar site (Station B).

For radio-relay paths exceeding 10 km, obstacle elevations are calculated using the equivalent Earth radius rather than the actual Earth radius. The equivalent Earth radius, R_e (km), is defined in [25] and obtained from (1):

$$R_e = k \cdot R_0 \tag{1}$$

where R_0 (km) is the actual Earth radius, $R_0 = 6378$ km and k is refractive factor (tropospheric factor). The value of the refraction factor k is variable and depends on the season, temperature variations, altitude, section length [22]. The mean value applied in calculations for the European mainland is $k = 4/3$, under standard atmospheric conditions. Due to the short length of the considered link (3.57 km), the effect of Earth curvature is negligible and does not significantly influence the propagation path.

The main requirement for radio-relay link operation is the existence of LoS between the antennas of Station A and B. In addition to LoS, Fresnel zone clearance must also be verified to ensure unobstructed electromagnetic wave propagation. Obstructions within the first Fresnel zone may introduce diffraction losses and degrade link performance. LoS between the antennas exists if the following condition in (2) is satisfied, according to [25]:

$$h = h_A \cdot \frac{d_2}{d} + h_B \cdot \frac{d_1}{d} - q - y \tag{2}$$

where h_A, h_B (m) are elevation of the antenna center at stations A and B, d_1, d_2 (km) are distances to the obstacle from stations A and B, d is horizontal distance between the stations A and B, q (m) is obstacle elevation, y (m) is Earth curvature correction.

The terrain profile and locations of the radio relay stations were determined using Digital Terrain Model (DTM) data, as shown in Fig. 1. Radio relay station parameters are given in Tab. 1.

In addition to LoS conditions, unobstructed electromagnetic wave propagation must also be ensured. This

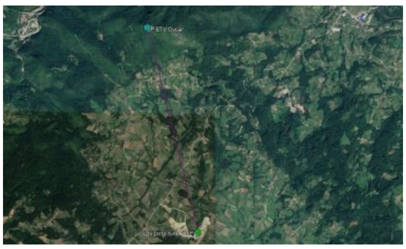

Fig. 1. Geographical locations of the radio relay stations.

Parameter [m]	**Station A – Laz**	**Station B – Ovcar**
Latitude	43°51′53.21″ N	43°53′46.74″ N
Longitude	20°13′37.39″ E	20°13′01.36″ E
Ground elevation	455 m	964 m
Antenna height above ground	19 m	20 m

Tab. 1. Radio relay station site parameters.

requirement is satisfied when the first Fresnel zone remains completely free of obstacles along the propagation path. The radius of the first Fresnel zone at any point along the path is determined using (3) according to [26]

$$r = 31.6 \cdot \sqrt{\lambda \cdot \frac{d_1 \cdot d_2}{d_1 + d_2}} \tag{3}$$

where r (m) is radius of the first Fresnel zone and λ is wavelength, for the required frequency.

The distances d_1 and d_2 are mutually dependent, since their sum corresponds to the total length of the radio-relay link.

Based on the considered link distance, operating frequency, and antenna heights of 20 m and 19 m, the maximum radius of the first Fresnel zone can be obtained by determining the maximum value of (4)

$$r = 17.32 \cdot \sqrt{\frac{d}{4 \cdot f}} \, . \tag{4}$$

The analysis indicates that the maximum radius of the first Fresnel zone is 4.2 m, while the Fresnel ellipsoid, neglecting terrain morphology and obstacles, extends approximately 16 m above the ellipsoid reference surface.

The horizontal distance between the two radio relay stations was calculated without considering Earth curvature or the elevation difference between Laz and Ovcar site, but rather as the direct horizontal separation between the locations. The horizontal distance between the sites is obtained by (5)

$$d_H = d \cdot \cos(\alpha\left[\text{rad}\right]). \tag{5}$$

The horizontal distance between radio relay stations Laz and Ovcar denoted as d_H, is 3.57 km. The spatial distance between the antennas at radio relay stations, taking into account the elevation angle, is $d = 3.58$ km. The distance between the Laz and Ovcar locations, considering the terrain profile, is 3.69 km.

The antenna azimuths are defined as deviations from north. The elevation angles of the antennas are given by the following expressions (6), (7):

$$\alpha = \text{arctg}\left(\frac{h_A - h_B}{d_H}\right), \tag{6}$$

$$\beta = \text{arctg}\left(\frac{h_B - h_A}{d_H}\right) \tag{7}$$

where α, β (°) are elevation angles at stations A and B, h_A is antenna elevation at Station A, h_B is antenna elevation at Station B, d_H is the distance between radio-relay Stations A and B.

The azimuths of the antenna orientations and the antenna elevation angles at radio-relay Stations A and B are given in Tab. 2.

Narrow beamwidths demand precise mechanical tilting and accurate pointing for reliable reception, for antenna elevation angle of about 8° at 15 GHz. Linking the calculated elevation angles to the actual physical alignment provides valuable guidance for minimizing signal degradation under real mountainous conditions.

Based on [23], [24], the route along which the digital radio-relay link is planned to be implemented is located in an area characterized by the following environmental link quality analysis conditions, shown in Tab. 3.

The link budget represents a fundamental tool for evaluating system performance and includes all relevant gains and losses along the propagation path. The quality of a digital radio relay link is primarily determined by the received signal level, propagation losses, antenna gains, and the available fading margin. These parameters define the reliability and performance of the system under real operating conditions. The received signal level is initially evaluated under non-fading conditions and calculated according to standard link-budget methodology [2], [3] as in (8):

$$P_r = P_t - A \tag{8}$$

where P_t (dBm) is the transmitted power and A represents the total propagation attenuation. The total path attenuation is defined as the difference between total propagation losses and the overall antenna gain [20], [25] and calculated in (9):

$$A = A_t - G_{uk} \tag{9}$$

where A_t (dB) includes all propagation-related losses, and G_{uk} (dB) represents the total antenna gain.

Station	Azimuth to other station (°)	Elevation angle to other station (°)
A (Laz)	347.75 → B (Ovcar)	8.124
B (Ovcar)	167.75 → A (Laz)	–8.147

Tab. 2. Antenna azimuths and elevation angles at radio-relay Stations A and B.

Parameter	Value
Average air temperature	15°C
Average atmospheric pressure	1013 hPa
Average water vapor density (worst month)	15.0 g/m³
Absolute humidity	0.320 g/m³

Tab. 3. Parameters of the radio-relay link environment.

The total attenuation consists of multiple components, including free-space path loss, diffraction losses due to terrain obstacles, atmospheric absorption, losses introduced by system components (waveguides, cables, filters, connectors), additional implementation and tolerance losses. The free-space path loss depends on the link distance and operating frequency and is given by (10), according to [20]:

$$A_0 = 92.4 + 20\log_{10} d + 20\log_{10} f \tag{10}$$

where d (km) is the link distance and f (GHz) is the operating frequency. This expression is valid under far-field conditions.

The total gain of the parabolic antennas is defined as the sum of the antenna gains at both ends of the link, reduced by the attenuation introduced by the radomes. The gain is expressed relative to an isotropic radiator and can be calculated as follows (11), according to standard antenna-gain relations [3]:

$$G_{uk} = G_A + G_B - A_{rdA} - A_{rdB} \tag{11}$$

where G_A (dBi) is the gain of the parabolic antenna at the radio relay Station A (Laz), G_B (dBi) is the gain of the parabolic antenna at the radio relay Station B (Ovcar), A_{rdA} (dB) is the radome attenuation at the antenna at the radio relay Station A, A_{rdB} (dB) is the radome attenuation at the antenna at the radio relay Station B.

The gain of a parabolic antenna depends on its diameter and the operating frequency of the digital radio-relay link. It is expressed relative to an isotropic radiator and can be calculated using the following expression (12), according to classical parabolic antenna theory [3]:

$$G = 17.8 + 20\log_{10} D + 20\log_{10} f \tag{12}$$

where G (dBi) represents the gain of the parabolic antenna relative to an isotropic radiator, D (m) is the antenna diameter, and f (GHz) is the operating frequency.

The terrain profile and Fresnel zone clearance are illustrated in Fig. 2, confirming unobstructed propagation conditions along the link.

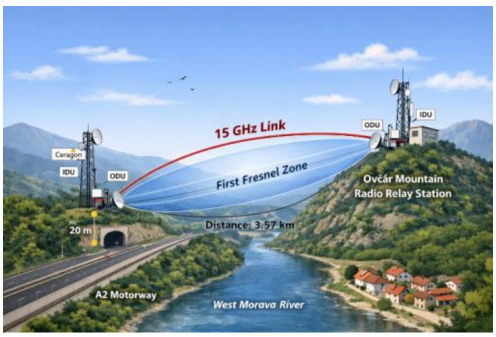

Fig. 2. Terrain profile and first Fresnel zone clearance for the 15 GHz radio relay link between the Laz tunnel and the Ovcar site, showing clear LoS conditions and unobstructed propagation.

To ensure reliable operation, a fading margin must be defined to compensate for signal level variations caused by multipath propagation and environmental effects [25]. It is calculated as in (13):

$$A_{\mathrm{fr}} = P_{\mathrm{r}} - P_{\mathrm{P}} \tag{13}$$

where P_{P} (dBm) is absolute receiver threshold level defined for a corresponding bit error ratio (BER).

In practical systems, interference from nearby radio systems may degrade the receiver sensitivity. Therefore, the effective fading margin is reduced as (14):

$$A_{\mathrm{fri}} = A_{\mathrm{fr}} - A_{\mathrm{C/I}} \tag{14}$$

where $A_{\mathrm{C/I}}$ (dB) represents degradation of the receiver threshold for a given carrier-to-interference ratio (C/I).

Due to the analyzed short path length, Earth curvature effects are negligible and do not introduce additional propagation losses. The propagation environment is further characterized by moderate climatic conditions, with a rain rate of 31.46 mm/h (0.01% of time), corresponding to climatic zone *K* [22].

The design procedure starts with the definition of the input system and environmental parameters. The proposed propagation-aware radio-relay link design methodology consists of ten sequential steps, as illustrated in Fig. 3. These include the selected frequency band, link distance, required transmission capacity, target availability, and terrain data describing the geographical area of interest. These parameters establish the initial design requirements and provide the basis for all subsequent propagation, availability, and link-budget calculations. In the first step, a detailed terrain profile is extracted from digital terrain data. This step is addressed in Sec. 2.1. The obtained profile is used to verify line-of-sight conditions between the candidate radio-relay sites and to identify potential terrain obstructions along the propagation path. The influence of Earth curvature is also considered through the effective Earth-radius approach, allowing a realistic assessment of path geometry under standard atmospheric conditions. Based on the terrain profile, line-of-sight conditions, and obstacle clearance, an initial feasibility assessment of the radio-relay path is performed [18, 19, 25].

Step 2 focuses on Fresnel-zone analysis and antenna configuration optimization. The analytical relations used in this step are presented in Sec. 2.1. The radius of the first Fresnel zone is calculated along the propagation path and used to verify that sufficient clearance is maintained above terrain obstacles. Potential obstructions within the Fresnel zone are identified and assessed because they may introduce diffraction losses and degrade link performance. Based on the obtained clearance conditions, the required antenna heights are evaluated and, if necessary, adjusted to ensure reliable propagation and compliance with the recommended Fresnel-zone clearance criteria. This step is particularly important for minimizing diffraction effects and achieving the fade margin required for high-availability radio-relay operation [25], [26].

Step 3 addresses the evaluation of the propagation losses affecting the radio-relay link. The propagation-loss calculations used in this step are presented in Sec. 2.1. The free-space path loss is first calculated as a function of the operating frequency and propagation distance. Additional attenuation mechanisms, including diffraction loss caused by terrain obstructions and clutter- or terrain-related losses, are then considered to obtain a more realistic representation of the propagation environment. The individual loss components are combined to determine the total propagation loss, which represents one of the key parameters for subsequent link-budget calculations and received signal level estimation. Accurate evaluation of these losses is essential for reliable prediction of link performance and availability in complex propagation environments [20, 25, 26].

Step 4 involves the characterization of environmental conditions and the evaluation of atmospheric attenuation mechanisms affecting radio-wave propagation. The atmospheric attenuation models introduced in this step are used in the outage-probability analysis presented in Sec. 3. The relevant climatic and meteorological parameters, including temperature, atmospheric pressure, humidity, water-vapor density, and regional rainfall characteristics, are first determined for the considered propagation environment [24], [25]. Based on these parameters, attenuation due to gaseous absorption by oxygen and water vapor is evaluated using the corresponding ITU-R models [27]. In addition, attenuation caused by precipitation, including rain effects, is estimated using regional rainfall statistics and frequency-dependent attenuation coefficients [23], [29]. The impact of clouds and fog is also considered, particularly under adverse weather conditions where additional attenuation may occur [31]. At microwave frequencies, atmospheric effects significantly influence propagation. Therefore, accurate characterization of environmental conditions is essential for reliable loss estimation and availability prediction.

Step 5 involves the evaluation of geoclimatic parameters required for fading and outage prediction. The obtained geoclimatic parameters are later used in the outage probability calculations presented in Sec. 3.1 and 3.2. The geoclimatic factor is determined using regional climatic data, terrain characteristics, and atmospheric refractivity conditions. Particular attention is given to the refractivity gradient in the lower atmosphere, which directly influences the effective Earth-radius factor and the propagation characteristics of terrestrial microwave links. In addition, regional climatic conditions and worst-month statistics are analyzed because they provide the basis for predicting the occurrence of severe propagation impairments and fading events. The obtained geoclimatic parameters are subsequently used for outage probability calculations and link-availability assessment in accordance with ITU-R recommendations [22], [25].

Step 6 focuses on the assessment of multipath propagation effects and fading statistics. The fading and outage prediction procedures are described in Sec. 3.1–3.3. Both flat (non-selective) and selective fading mechanisms are analyzed because they represent the dominant sources of signal degradation in terrestrial microwave radio-relay systems. The statistical distribution of fade depth is evaluated using ITU-R prediction procedures, while the multipath occurrence factor is determined from the previously calculated geoclimatic parameters. For selective fading analysis, the signature curve method is applied to estimate the probability that the bit error ratio exceeds the specified performance threshold under multipath conditions. The combined analysis of fade-depth distribution, multipath occurrence statistics, and selective fading characteristics provides the basis for predicting outage probability and evaluating the reliability of the radio-relay link under realistic propagation conditions [21, 25, 35].

Step 7 consists of availability and outage performance evaluation. Availability assessment is presented in Sec. 4. Annual availability is calculated by combining the contributions of the dominant propagation impairment mechanisms identified in the previous steps. The outage probability associated with multipath fading is first estimated using the geoclimatic parameters, fade-depth statistics, and worst-month prediction procedures recommended by the ITU-R [25]. Subsequently, the contribution of rain-induced attenuation to link unavailability is evaluated using regional rainfall characteristics and frequency-dependent attenuation models [23, 25, 29]. The individual outage contributions resulting from multipath propagation and precipitation effects are then combined to determine the overall annual availability of the radio-relay link. This step provides the principal performance indicator used to assess system reliability and to verify whether the designed radio-relay link satisfies the required service-availability objectives and quality-of-service requirements [23, 25, 29].

Step 8 provides verification of the analytical results using the Radio Mobile software tool [39]. The verification procedure is presented in the first part of Sec. 5. The analysis is performed using the same geographical coordinates, terrain profile, antenna heights, antenna characteristics, operating frequency, and propagation path parameters adopted in the analytical assessment. The generated terrain profile is used to verify line-of-sight conditions and confirm adequate Fresnel-zone clearance along the entire radio-relay path. Furthermore, terrain-aware propagation analysis is conducted to estimate the received signal level and overall path performance under realistic environmental conditions. The obtained results are subsequently compared with the analytical predictions, providing an independent consistency assessment. This comparison provides additional confidence in the analytical assessment and demonstrates the practical applicability of the proposed radio-relay link design procedure [25], [39].

Step 9 provides the final evaluation of the radio-relay link performance. The corresponding link-performance results are discussed in the subsequent part of Sec. 5. The received signal level is determined using the calculated link budget and compared with the receiver sensitivity threshold in order to verify adequate signal reception under

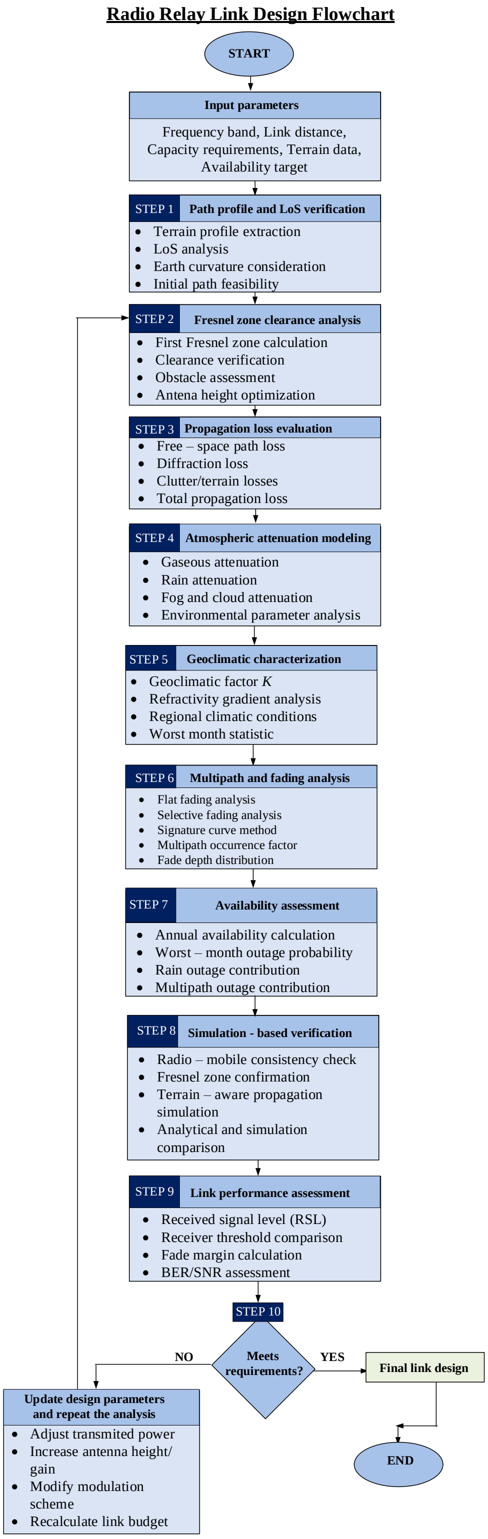

Fig. 3. Flowchart illustrating the proposed propagation-aware radio relay link design methodology.

normal operating conditions. The previously evaluated Fresnel-zone clearance and propagation losses are taken into account when assessing the overall link performance. Based on the difference between the received signal level and the receiver threshold, the available fade margin is calculated and used as an indicator of the link robustness against propagation impairments. In addition, signal-to-noise

Parameter / Concept	Symbol	Unit	Description
Frequency band	15	GHz	Operating frequency
Channel bandwidth	28	MHz	Duplex channel bandwidth
Link distance (horizontal)	3.57	km	Horizontal distance between sites
Link distance (slant)	3.58	km	Spatial distance between antennas
Antenna diameter	0.3	m	Parabolic antenna size
Antenna heights	19 / 20	m	Laz / Ovcar site
Antenna gain	30.86	dBi	Gain per antenna
Transmitted power	22	dBm	Maximum transmitter output
Received signal level	–44.28 / –43.81	dBm	Ovcar-Laz site
Fade margin	18.72 / 19.19	dB	Ovcar / Laz site
Polarization	Vertical	-	Signal polarization
Fresnel zone radius (max)	4.2	m	First Fresnel zone (mid-path)
Rain rate (0.01%)	31.46	mm/h	(Zone *K*) [22]
Configuration	1+0	-	System architecture
Capacity	100	Mb/s	Transmission capacity

Tab. 4. Key parameters of the analytical radio relay link design stage.

ratio (SNR) and bit error rate (BER) performance are evaluated to confirm that the selected modulation scheme and transmission parameters satisfy the required quality-of-service criteria. This step provides a comprehensive assessment of link reliability and verifies whether the designed system fulfills the specified technical and operational requirements [25, 33, 34].

Finally, Step 10 performs the final design verification and decision process. The calculated availability, fade margin, received signal level, BER performance, and other key system parameters are compared with the predefined design requirements. If all performance objectives are satisfied, the radio-relay link configuration is accepted as the final design solution. Otherwise, the design parameters, such as antenna height, antenna gain, transmitted power, modulation scheme, or other system characteristics, are adjusted and the entire assessment procedure is repeated. This iterative approach ensures that the final radio-relay link design achieves the required reliability, availability, and quality-of-service targets under the considered propagation conditions [25].

The subsequent sections describe the individual workflow steps presented in Fig. 3 and explain the corresponding analytical procedures, propagation analyses, availability calculations, verification process, and link-performance assessment.

The main parameters of the analyzed radio relay link are summarized in Tab. 4.

3. Probability of Outage in Radio Relay Links

The design of line-of-sight (LoS) radio relay systems requires careful consideration of various propagation effects that can degrade signal quality and lead to link outages. Reference [25] provides standardized methods for predicting these effects and estimating the availability and reliability of terrestrial microwave links. Several propagation phenomena must be considered in LoS radio relay design: diffraction fading due to terrain obstacles or partial obstructions, atmospheric gas attenuation (oxygen and water vapor absorption), multipath fading caused by reflections and atmospheric layering, beam spreading and defocusing due to refractive index variations, attenuation due to precipitation (rain, snow, hail) and atmospheric particles, variations in angle of arrival and departure due to refraction reduction of cross-polarization discrimination (XPD), signal distortion due to frequency-selective fading and delay spread. These mechanisms contribute to total propagation loss and directly impact link availability. Total propagation loss consists of multiple contributions, including free-space loss, atmospheric gas attenuation, diffraction loss, multipath fading effects, and rain attenuation. Unless otherwise stated, the outage prediction equations presented in this section are adopted from the relevant ITU-R recommendations, primarily [21], [25] and [29]. Atmospheric gas attenuation [27] becomes significant above 10 GHz and is calculated as (15):

$$A_a = \gamma_a \cdot d \quad [\text{dB}] \tag{15}$$

where γ_a (dB/km) is the specific gaseous attenuation and A_a is the total gaseous attenuation along the propagation path. The specific attenuation γ_a is calculated in accordance with [27], as follows (16):

$$\gamma_a = (\gamma_0 - \gamma_w) \tag{16}$$

where γ_0 (dB/km) is specific attenuation due to dry air and γ_w (dB/km) is specific attenuation due to the presence of water vapor in the air.

The attenuation due to gaseous absorption is calculated under standard environmental conditions: air temperature of 15°C, atmospheric pressure of 1013 hPa, and a water vapor density of 15.0 g/m³ ([25], for the worst month). For long paths at frequencies above 20 GHz, it is advisable to consider the statistical distribution of water vapor density and ambient temperature along the propagation path. Information on water vapor density is provided in [25]. However, in this case, the use of a standard value of 7.5 g/m³ has a negligible impact on the accuracy of the calculation.

Variations in atmospheric refractivity conditions cause changes in the effective Earth radius or the *k*-factor from its mean value, which is approximately 4/3 for a standard atmosphere [22]. When the atmosphere becomes sufficiently refractive (large positive values of the refractive index gradient and a reduced value of the *k*-factor), the propagation path of the radio beam is bent such that the Earth appears as an obstacle along the direct path between the transmitter and receiver, leading to an increase in a type of fading known as diffraction fading. This type of fading is a key factor in determining antenna heights.

The statistics of the *k*-factor for a given location can be determined by measurement or by predicting the refractive index gradient in the lowest 100 m of the atmosphere [22]. These gradients must be averaged to obtain an effective *k*-factor value, k_e, for the path lengths of interest. Values of k_e exceeded for 99.9% of the time are discussed in terms of path clearance criteria. Diffraction loss can be approximated according to [26] as in (17):

$$A_d = -20h/r + 10 \quad [\text{dB}] \tag{17}$$

where h [m] is the height difference between the most significant obstacle along the path and the propagation trajectory (h is negative if the top of the obstacle lies above the line-of-sight path), and r is the radius of the first Fresnel ellipsoid.

At the frequencies above 2 GHz, diffraction fading has traditionally been mitigated by installing antennas at sufficiently high elevations, such that even the most severe beam bending would not place the receiver within the diffraction region when the effective Earth radius is reduced below its nominal value. Diffraction theory indicates that the direct path between the transmitter and receiver requires a clearance above ground level of at least 60% of the first Fresnel zone radius in order to achieve free-space propagation conditions. More recently, with improved understanding of this mechanism and the availability of statistical data for the effective Earth radius factor k_e, which enables statistical predictions, some have adopted antenna heights that result in very low but well-defined outage probabilities.

Various fading mechanisms caused by highly refractive atmospheric layers must be considered when planning links longer than a few kilometers. These include beam spreading (also known as defocusing), antenna decoupling, multipath propagation due to surface reflections, and multipath propagation caused by atmospheric effects. Most of these mechanisms may occur individually or in combination with others. A pronounced form of frequency-selective fading occurs when the direct signal beam combines with a surface-reflected signal, resulting in multipath fading. Small-scale fading due to atmospheric turbulence is always present in conjunction with these mechanisms; however, at frequencies below 40 GHz, its impact on the overall fading distribution is negligible.

The method for predicting the fading distribution at a single frequency (or over a narrowband channel) for large fade depths in the average worst month, applicable worldwide, does not require the path profile and can be used for initial planning, licensing, or design purposes. A second method is applicable to all fade depths and combines the large fade-depth prediction method with an interpolation procedure for shallow fading. The method for predicting signal enhancement uses the fade depth predicted by the small percentage of time method as the only input parameter.

3.1 Predicting Outage Probability for Small Percentages of Time

For small percentages of time, the following calculation procedure is applied. For the paths of interest, the geoclimatic factor K corresponding to the average worst month should be determined based on available fading data. In the absence of measured data, and when detailed link design is required, the geoclimatic factor for the average worst month should be calculated using the following expression (18), according to [25]:

$$K = 10^{-4.4-0.0027 dN_1} \cdot (10 + S_a)^{-0.46} \tag{18}$$

where dN_1 represents the refractivity gradient in the lowest 65 m of the atmosphere that is not exceeded for 1% of an average year, and S_a denotes the terrain roughness. The parameter dN_1 is provided on a global grid of 1.5° latitude and longitude resolution in [22]. The appropriate value at the path center should be obtained by bilinear interpolation from the four nearest grid points. These data are available in tabular form from the Radio-communication Bureau (BR).

The parameter S_a [m] is defined as the standard deviation of terrain elevation over an area of 110 km × 110 km with a resolution of 30 seconds. The area should be aligned with longitude such that it is symmetrically distributed around the meridian passing through the path center. For rapid estimation of K in planning applications, an approximate expression given in [25] may be used in (19):

$$K = 10^{-4.6-0.0027 dN_1} . \tag{19}$$

Based on the antenna heights h_e and h_r (m), the path inclination angle is determined according to [25] in (20):

$$\begin{aligned} |\varepsilon_p| &= |h_r - h_e| / d \quad [\text{mrad}], \\ h_c &= \frac{h_r + h_e}{2} - \frac{d^2}{102} - h_t \end{aligned} \tag{20}$$

where h_t is mean terrain elevation along the path, including vegetation and d (km) is the path length.

The percentage of time p_w exceeded in the average worst month is calculated according to [25] using (21):

$$p_w = Kd^{3.51}(f^2+13)^{0.447} \cdot 10^{-0.376\tanh\left(\frac{h_c-147}{125}\right) - 0.334|\varepsilon_p|^{0.39} - 0.00027 h_L + 17.85 v_{sr} - A/10} \quad [\%] \tag{21}$$

where v_{sr} denotes the sub-refractive parameter (22), where the sub-refractive parameter is defined in [25]:

$$v_{sr} = \min\left\{\left(\frac{dN_{75}}{50}\right)^{1.8} \exp\left[-\frac{h_c}{2,5\sqrt{d}}\right], v_{sr\,limit}\right\} \qquad (22)$$

subject to the upper limit (23):

$$v_{sr\,limit} = \frac{dN_{75}\cdot d^{1.5}\cdot f^{0.5}}{24730}\ [m] \qquad (23)$$

where $v_{sr\,limit}$ is an empirical prediction parameter exceeded for 1% of the time in the average worst month within the lowest 75 m of the atmosphere. The overall standard deviation of the prediction error associated with these expressions is approximately 5.2 dB, including year-to-year variability, while the mean prediction error is less than 3 dB.

3.2 Predicting Outage Probability for All Percentages of Time

The method applicable to all percentages of time for predicting the percentage of time during which any fade depth is exceeded combines the fade depth distribution obtained from the calculation for small percentages of time with an empirical interpolation procedure for shallow fading extending down to 0 dB.

Using the method for small percentages of time, the multipath occurrence factor p_0 can be calculated as in (24) according to [25], representing the outage distribution for deep fading with the percentage of time:

$$p_0 = K\cdot d^{3.51}\left(f^2+13\right)^{0.447}\cdot 10^{-0.376\tanh\left(\frac{h_c-147}{125}\right)-0.334|\varepsilon_p|^{-0.39}-0.00027h_L+17.85v_{sr}}\ [\%]. \qquad (24)$$

It should be noted that equation (21) is equivalent to (24) for $A = 0$.

Equations (25–30) follow the interpolation procedure recommended in [25].

The fade depth A_t, at which the transition between the deep fading distribution and the shallow-fading distribution occurs, is determined using (25):

$$A_t = 25 + 1.2\cdot\log_{10} p_0\ [\%]. \qquad (25)$$

The subsequent procedure depends on whether the required fade depth A is greater or less than A_t. If the required fade depth A is greater than or equal to A_t, the percentage of time during which A is exceeded in the average worst month is given by (26):

$$p_w = p_0\cdot 10^{-A/10}\ [\%]. \qquad (26)$$

If the required fade depth A is less than A_t, the empirical interpolation procedure is applied in (27):

$$p_t = p_0\cdot 10^{-A_t/10}. \qquad (27)$$

Equation (27) is consistent with (21), as appropriate, for $A = A_t$. First, q_a' is calculated based on the variation in fade depth A_t and the corresponding percentage of time p_t: as (28):

$$q_a' = -20\log_{10}\left\{-\ln\left[100-p_t\right]/100\right\}/A_t. \qquad (28)$$

Then, q_a is obtained for the required fade depth A (29):

$$q_a = 2+\left[1+0.3\cdot 10^{-A/20}\right]\left[10^{-0.016\cdot A}\right]\left[q_t+4.3\cdot\left(10^{-A/20}+A/800\right)\right]. \qquad (29)$$

Finally, the percentage of time p_w for which a fade depth A(dB) is exceeded in the average worst month is calculated as (30):

$$p_w = 100\left[1-\exp\left(-10^{-q_a A/20}\right)\right].\ [\%] \qquad (30)$$

Provided that $p_0 > 2000$, the above procedure yields a monotonic relationship between p_w and A, which can be used to determine A for a given value of p_w through a simple iteration.

The method extended to all percentages of time provides a continuous statistical representation of fading behavior by combining deep fading distributions with interpolation toward shallow fading conditions. This ensures a consistent description of signal variability across the entire dynamic range.

The obtained results indicate that moderate fading events significantly influence overall system performance, particularly under typical operating conditions. This highlights the importance of considering the full distribution, rather than focusing solely on extreme fading events.

Nevertheless, the interpolation approach introduces an inherent approximation, especially in the transition region near 0 dB, where physical propagation mechanisms are not explicitly modeled. Despite this limitation, the method remains sufficiently accurate for engineering applications and system-level performance evaluation.

3.3 Predicting Outage Probability from Non-Selective Fading

The outage probability, P_{ns} ,due to non-selective fading is calculated using (31), according to [25]:

$$P_{ns} = p_w/100 \qquad (31)$$

where p_w (%) denotes the percentage of time during which the flat fading margin $A = F$ (dB), corresponding to the specified BER, is exceeded in the average worst month. The flat fading margin F, obtained from the link budget and equipment specifications, also accounts for potential margin reduction caused by interference effects in practical link deployment scenarios.

3.3.1 Predicting Outage Probability in Unprotected Digital Systems from Selective Fading

Flat and selective fading are considered statistically independent and are therefore analyzed separately [21]. Various methods exist for predicting the degradation of radio-relay link performance due to selective fading; in this work, the signature curve method is adopted as a representative and widely used approach. The outage probability is defined as the probability that the BER exceeds a specified threshold at the receiver.

The significant delay time is estimated according to [21], using (32):

$$\tau_{\mathrm{m}} = 0.7 \cdot \left(\frac{d}{50}\right)^{1.3} [\mathrm{ns}] \tag{32}$$

where d (km) denotes the path length.

Subsequently, the multipath activity parameter η is evaluated according to (33), given in [21]:

$$\eta = 1 - \exp\left(-0.2 \cdot P_0^{0.75}\right) \tag{33}$$

where $P_0 = p_{\mathrm{w}} / 100$ represents the multipath occurrence factor corresponding to the percentage of time p_{w} (%) during which the fade margin $A = 0$ dB is exceeded in the average worst month.

The outage probability due to selective fading in an unprotected system, denoted as P_{s}, is calculated using (34). The signature curve approach described in [21] is used.

$$P_{\mathrm{s}} = 2.15 \cdot \eta \cdot \left(W_{\mathrm{M}} \cdot 10^{-B_{\mathrm{M}}/20} \cdot \frac{\tau_{\mathrm{m}}^2}{|\tau_{\mathrm{r,M}}|} + W_{\mathrm{M}} \cdot 10^{-B_{\mathrm{NM}}/20} \cdot \frac{\tau_{\mathrm{m}}^2}{|\tau_{\mathrm{r,NM}}|} \right) \tag{34}$$

where W_{x} (GHz) represents the signature width, B_{x} (dB) denotes the signature depth, and $t_{\mathrm{r,x}}$ (ns) is the reference delay used to derive the signature, with x indicating either minimum-phase (M) or non-minimum-phase (NM) fading conditions.

If only the normalized system parameter K_{n} is available, the outage probability due to selective fading can alternatively be estimated using (35), using the signature curve approach described in [21]:

$$P_{\mathrm{s}} = 2.15 \cdot \eta \cdot \left(K_{\mathrm{n,M}} + K_{\mathrm{n,NM}}\right) \cdot \frac{\tau_{\mathrm{m}}^2}{T^2} \tag{35}$$

where T (ns) denotes the symbol duration, and $K_{\mathrm{n.x}}$ represents the normalized system parameter corresponding to either minimum-phase or non-minimum-phase fading.

Signal attenuation may also arise from absorption and scattering caused by hydrometeors such as rain, snow, hail, and fog. While rain attenuation can generally be neglected at frequencies below 5 GHz, it must be explicitly considered at higher frequencies, where its impact increases significantly. For propagation paths located at high latitudes, or at high altitudes in lower-latitude regions, wet snow may also produce considerable attenuation over a broad frequency range. At frequencies where both rain attenuation and multipath fading are significant, the corresponding exceedance probabilities for a given fade depth must be combined to obtain an accurate estimation of overall signal degradation.

Long-term statistics of rain-induced attenuation can be evaluated using a simplified approach. The rain rate $R_{0.01}$, corresponding to 0.01% of the time with a one-minute integration period, should be obtained from local measurements or, if unavailable, from [29]. The specific attenuation g_{R} (dB/km) is then determined for the considered frequency, polarization, and rain rate using [29], according to the power-law relationship (36):

$$g_{\mathrm{R}} = k \cdot R^{a} \tag{36}$$

where k and a are frequency-dependent coefficients defined for linear (horizontal and vertical) polarization over terrestrial paths. The corresponding regression coefficients are provided in the [29].

The total outage probability due to rain is evaluated by considering the dominant contribution among rain-induced errors, combined precipitation effects, and polarization impairments, as obtained from the previously described methods.

Prediction methods for digital systems have evolved from defining outage probability as the probability that BER exceeds a specified threshold ($1 \cdot 10^{-3}$), in accordance with [32] requirements.

While clear-air effects predominantly impact error performance and precipitation primarily affects availability, practical systems exhibit mutual interactions. Specifically, clear-air propagation mechanisms may contribute to availability degradation, whereas rain-induced effects can also influence error performance. Therefore, a comprehensive assessment of link reliability requires simultaneous consideration of both mechanisms within a unified framework.

The recommendation [25] provides a comprehensive framework for predicting propagation impairments and estimating outage probability in radio relay systems. By incorporating diffraction, multipath fading, atmospheric absorption, and rain attenuation, engineers can design reliable radio relay links that meet availability requirements. Accurate prediction of outage probability is essential for ensuring system performance, especially in high-frequency and long-distance links where propagation effects are more pronounced. Obtained results in this research are consistent with the findings of Olsen and Tjelta, whose work significantly contributed to the development of ITU-R multipath fading prediction models for terrestrial LoS links [35].

4. Radio Relay Link Availability

The total availability of a radio relay link is given by (37–38), according to [34]:

$$R_a = 100 - N, \tag{37}$$

$$N = N_a + \sum N_{pr} \tag{38}$$

where R_a (%) is radio relay link availability, N (%) represents radio relay link unavailability, N_a (%) unavailability due to equipment failures, N_{pr} (%) is unavailability due to radio wave propagation effects.

For systems without redundancy or diversity techniques, unavailability is calculated using the following expression (39):

$$N_a = 2 \cdot s \cdot (N_1 + N_2) + (s+1) \cdot N_4 + 2 \cdot N_5 \tag{39}$$

where s is number of sections, N_1, N_2 are transmitter and receiver unavailability, N_4 is power supply unavailability and N_5 presents modulator/demodulator unavailability.

Error performance standards are defined according to [33]. The error performance objective (EPO) is calculated according to (40):

$$\text{EPO} = B_j \cdot (L_{link} / L_R) + C_j \tag{40}$$

where L_R = 2500 km is the reference length, L_{min} = 50 km is the minimum link length used for scaling the objectives with the practical link length L_{link}, B_j is the performance coefficient corresponding to the selected error performance parameter, and C_j is the corresponding correction factor. EPO values for access and short sections of the hypothetical reference path (HRP) and hypothetical reference connection (HRC) can be applied only to assigned block allocations specified in [34], and for long network sections where allocation is based on distance and the portion of the allowed fixed block. For short network sections shorter than 50 km, EPO values for SDH systems designed according to [33] should be used.

Availability (or unavailability) and mean time between failures (MTBF) are calculated according to [34], using the same division of the national portion of the HRP or HRC. Availability standards apply to each transmission direction of fixed wireless links within access and short network sections of international digital paths with constant transmission rates, assuming allocation is based on fixed blocks. The availability AR and mean outage M_0 for a link of length L_{link} can be calculated using (41–42), according to [34]:

$$\text{AR} = 1 - \left(B_j \cdot \frac{L_{link}}{L_R} + C_j \right), \tag{41}$$

$$M_0 = \frac{1}{\text{OI}} = \frac{1}{D_j \cdot \frac{L_{link}}{L_R} + E_j} \tag{42}$$

where j = 6 for national short-haul sections, and the parameter OI refers to the number of unavailability events per year. The reciprocal of M_0 should be multiplied by the number of seconds in a year to represent the effective significant time between unavailability events. For short network sections, the parameters in (41) and (42) are $C_j = 4 \cdot 10^{-4}$, $D_j = 0$, $E_j = 120$.

5. Link Budget Analysis

The link budget analysis was performed for the bidirectional radio relay link between the Laz tunnel (Station A) and the Ovcar site (Station B), following the propagation-aware methodology presented in the previous sections. The primary link design, propagation analysis, and availability assessment were performed analytically using the ITU-R-based methodology described in the previous sections.

The system operates using frequency division duplexing, where the lower-frequency channel is assigned to the Laz–Ovcar direction, while the higher-frequency channel is used for the reverse direction. Due to the absence of detailed information regarding neighboring systems and final frequency allocation, interference analysis was not explicitly included. However, sufficient frequency separation is assumed, ensuring negligible interference impact on overall system performance.

As the baseline configuration, the 32-QAM modulation scheme with a coding rate of 2/3 was selected. The selected modulation provides a compromise between spectral efficiency and propagation robustness, enabling the required transmission capacity of 100 Mb/s while maintaining sufficient resistance to fading and attenuation effects under the considered propagation conditions. In practical radio-relay systems, different modulation schemes may be employed depending on propagation conditions, receiver sensitivity requirements, and quality-of-service objectives. Lower-order modulation schemes generally improve robustness against fading and propagation impairments, whereas higher-order modulation schemes increase spectral efficiency and transmission capacity. Therefore, a qualitative comparison of several modulation formats that may be considered for the analyzed radio-relay link is presented in Tab. 5. The proposed propagation-aware assessment procedure is not restricted to the selected 32-QAM operating mode and may also be applied to alternative modulation schemes depending on system requirements and operating conditions.

Table 5 presents a numerical comparison of the supported modulation schemes for a 28 MHz channel operating in the 15 GHz frequency band. The receiver sensitivity and maximum transmission capacity values were taken from the manufacturer's specifications of the selected radio-relay equipment. The effective fade margins were calculated using the received signal levels obtained for the analyzed link while applying the same 16 dB receiver-

Modulation	Receiver sensitivity (dBm)	Required SNR (dB)	Fade margin (dB)	Maximum transmission capacity at 28 MHz (Mb/s)
QPSK	−89	6.5	28.72–29.19	43–52
16-QAM	−82.5	13	22.22–22.69	87–107
32-QAM	−79	16.5	18.72–19.19	115–140
64-QAM	−76	19.5	15.72–16.19	141–173

Tab. 5. Numerical comparison of modulation schemes for a 28 MHz channel in the 15 GHz frequency band.

threshold degradation due to interference as used for the reference 32-QAM configuration. Although the manufacturer specifies a maximum transmission capacity of 115 to 140 Mb/s for 32-QAM, the analyzed radio-relay link was designed to support the required user traffic capacity of 100 Mb/s.

The selected propagation model combines free-space attenuation with diffraction loss, refined subpath attenuation integration, and multipath propagation effects. Troposcatter attenuation is negligible due to the short path length, but was considered for completeness in accordance with ITU-R recommendations. Rain attenuation was evaluated using a rain intensity of 31.46 mm/h corresponding to the considered geographical region.

The calculated link budget results confirm that the designed radio relay link satisfies the performance and availability requirements of mission-critical TETRA communication systems. The obtained received signal levels remain well above the receiver sensitivity threshold, ensuring stable operation with sufficient fade margin in both transmission directions.

For a BER threshold of 10^{-6}, the calculated annual outage time is negligible, resulting in an availability of 99.999967%. Under worst-month propagation conditions, the availability decreases slightly to 99.995730%, corresponding to approximately 22 minutes of annual outage per year. Despite this reduction, the system maintains a very high level of operational reliability.

The calculated received signal levels are −43.81 dBm at the Ovcar site and −44.28 dBm at the Laz site, with corresponding fade margins of 19.19 dB and 18.72 dB, respectively. The obtained results indicate that the overall system availability remains above 99.99%, demonstrating satisfactory performance for the considered case study.

To assess the consistency of the analytical results, the considered radio-relay link was simulated using the Radio Mobile software tool (Fig. 4). The simulated propagation path was characterized by an elevation angle of 8.548°, a site elevation of 463.9 m, a total propagation loss of 127.6 dB, and a Fresnel-zone clearance of 50.36 m, confirming unobstructed line-of-sight propagation conditions. With a transmitter power of 22 dBm, the simulated received signal level was −45.9 dBm, showing good agreement with the analytical result presented in Tab. 7, with a difference below 2 dB.

The comparison showed good agreement between the analytical and simulation results for the terrain profile, line-of-sight conditions, Fresnel-zone clearance, and received signal level. Since field measurements and professional radio-planning tools were not available, the agreement between the analytical and simulation results should be interpreted as a consistency assessment rather than as full experimental validation of the proposed methodology. Additional attenuation caused by terrain morphology and clutter effects was negligible due to the short propagation path and favorable propagation conditions, and no significant increase in link unavailability was observed in either transmission direction.

Figure 5 illustrates the relationship between fade depth and the corresponding percentage of time exceeded. As expected, link availability increases with increasing fade margin, approaching near-ideal values for margins above 20 dB. The obtained results indicate that the analyzed system, with fade margins of approximately 18–19 dB, operates within a high-availability region, ensuring reliable performance under propagation conditions dominated by multipath fading and rain attenuation.

The presented case study demonstrates the applicability of the proposed assessment procedure under the considered propagation conditions rather than providing a statistical evaluation of multiple radio-relay links. Although the methodology was demonstrated on a single radio-relay link, it is based on established ITU-R propagation models and standard link-budget parameters, and its applicability to similar microwave radio-relay systems may be further investigated in future studies.

Good agreement between the analytical calculations and the Radio Mobile simulation results is shown in Tab. 6. The difference between the predicted received signal levels is 1.62 dB, which can be attributed to differences in propagation-model implementation, antenna parameters, and the use of nominal frequency values within the simulation environment. Despite these differences, both approaches predict comparable link performance and confirm the feasibility of the considered radio-relay path. The observed agreement therefore provides additional confidence in the consistency of the analytical assessment and the practical applicability of the proposed procedure. The main system and propagation parameters, calculated and simulated, are presented in Tab. 7. The calculated link budget results for both transmission directions are summarized in Tab. 8. The obtained results demonstrate the practical applicability of the proposed methodology for the considered case study and indicate that propagation-aware modeling can support reliable radio-relay link design in complex environment.

6. Conclusion

This paper presented a propagation-aware methodology for the design and evaluation of digital radio relay links in complex propagation environments. The proposed approach integrates terrain morphology, Fresnel zone clearance, atmospheric attenuation, rain effects, and multipath propagation into a unified analytical framework, enabling a more comprehensive assessment of propagation effects compared with simplified free-space-based approaches.

The proposed methodology was assessed through a case study of a 15 GHz LoS radio relay link between the Laz tunnel and the Ovcar site. The obtained results demonstrated good agreement between the analytical calculations and the Radio Mobile simulation, providing additional confidence in the consistency of the proposed methodology and supporting its practical applicability under realistic environmental conditions.

The performed analysis, based on ITU-R recommendations, showed that multipath fading represents the domi-

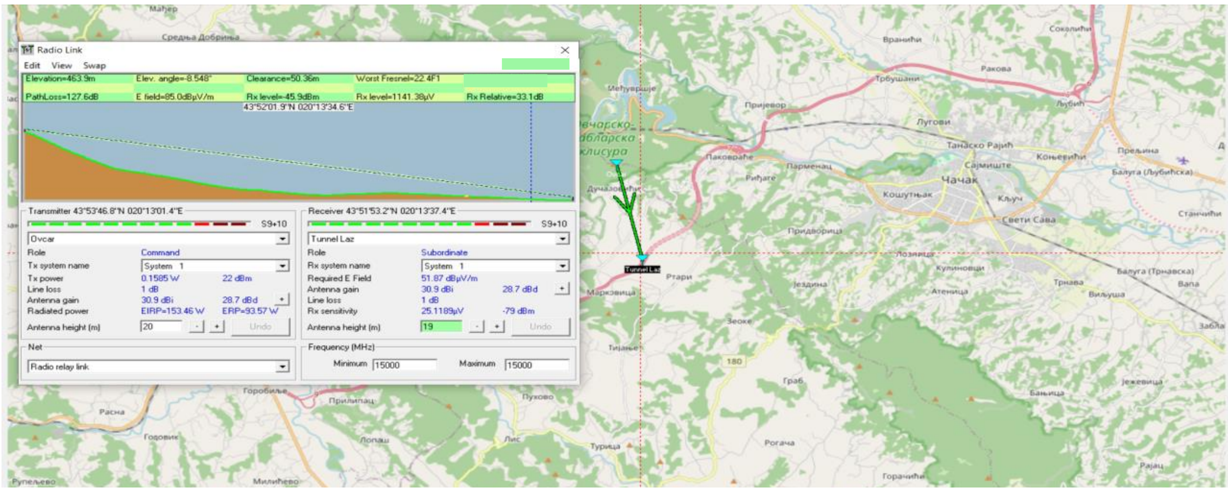

Fig. 4. Simulation-based propagation analysis of the 15 GHz Laz–Ovcar radio relay link obtained using Radio Mobile.

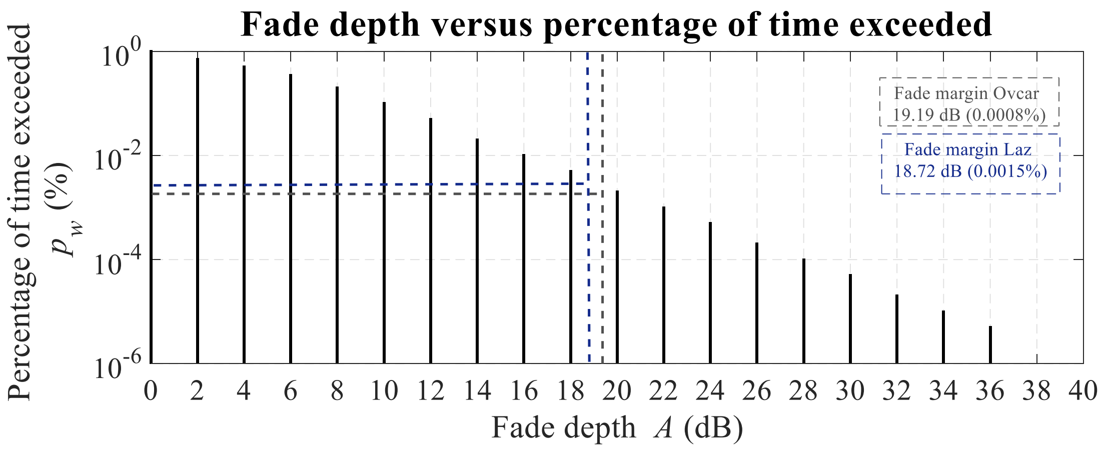

Fig. 5. Fade depth versus percentage of time exceeded for the analyzed 15 GHz radio relay link.

Parameter	Analytical calculation	Radio Mobile simulation
Frequency	15271 MHz	15000 MHz
Path distance	3.57 km	3.57 km
Antenna gain	32.7 dBi	30.9 dBi
Antenna height (Ovcar)	20 m	20 m
Antenna height (Laz)	19 m	19 m
Vertical angle	8.12°	8.54°
Received signal level (RSL)	–44.28 dBm	–45.90 dBm

Tab. 6. Comparison between analytical and simulation results.

PATH RADIO			
Station A		Station B	
Ovcar		Laz	
964.00 m (DTM altitude + clutter)		453.00 m (DTM altitude + clutter)	
Distance between stations: 3.57 km			
Station A (Calculations/Radio Mobile)		Station B (Calculations/Radio Mobile)	
Nominal power	22 dBm/22 dBm	Rx antenna attenuation	0.03 dB
Antenna attenuation (H)	0.03 dB	Threshold 10^{-3}	−82.50 dBm
Antenna attenuation (V)	0.00 dB	Threshold 10^{-6}	−79 dBm
Gain	32.7 dBi / 30.9 dBi	Gain	32.7 dBi / 30.9 dBi
Height of antenna	20.00 m / 20.00 m	Height of antenna	19.00 m / 19.00 m
Antenna azimuth	167.75°	Antenna azimuth	347.75°
Tx losses	2 dB / 1 dB	Rx losses	2 dB / 1 dB
EIRP (Equivalent isotropically radiated power)	184.92 W / 153.46 W	TD (losses)	0 dB
Parameters		Calculations	Radio Mobile
Frequency		15271 MHz	15000 MHz
Earth radius (land/sea)		8500 km	8500 km
Gas attenuation (15 g/m^3)		0.34 dB	Not explicitly modeled
Rain attenuation (31.46 mm/h)		5.9 dB	Not explicitly modeled
Power received		−44.28 dBm	−45.9 dBm
Diffraction attenuation		0 dB	0 dB
Reflection attenuation		0 dB	0 dB
Vertical angle		8.12°	8.54°

Tab. 7. Simulation and analytical input parameters for the Ovčar–Laz radio-relay link.

From	**To**	**Fade margin [dB]**	**P_R [dBm]**	**Operation mode**	**Link availability [%]**	**Outage duration [min]**	**Modulation scheme**	**Data rate [Mb/s]**
Laz (A)	Ovcar (B)	19.19	−43.81	LoS	99.999986	0	32-QAM	100
Ovcar (B)	Laz (A)	18.72	−44.28	LoS	99.999980	0	32-QAM	100

Tab. 8. Link budget results (annual conditions).

nant degradation mechanism for the considered short microwave link, while rain attenuation has a secondary impact that becomes more significant under worst-month propagation conditions. The achieved link availability exceeds 99.99%, satisfying the requirements of mission-critical TETRA communication systems.

Furthermore, the results indicate that 32-QAM can provide a suitable compromise between spectral efficiency and propagation robustness for the considered radio-relay link, while maintaining sufficient fade margin under the analyzed propagation conditions.

The presented results also demonstrate that realistic radio-relay link design cannot rely solely on simplified free-space propagation assumptions. Even under LoS conditions, accurate prediction of system performance requires detailed consideration of terrain morphology, atmospheric effects, and multipath propagation mechanisms. In this context, propagation-aware modeling represents a fundamental requirement for the reliable design of modern high-capacity microwave communication systems operating in realistic environments.

The presented study demonstrates a practical framework for propagation-aware assessment and design of radio-relay links in challenging propagation environments. The contribution of this work does not lie in the development of new propagation models or analytical expressions. Instead, it lies in the combined application of established ITU-R procedures within a structured assessment framework for complex propagation environments.

Future work will focus on experimental verification through field measurements in order to verify the obtained analytical and simulation-based results. Additional research will include the application of the proposed methodology to a larger set of radio-relay links characterized by different terrain profiles and propagation environments, enabling a broader statistical assessment of its applicability and robustness. Further extensions will include higher frequency bands, including millimeter-wave systems, as well as the investigation of adaptive modulation techniques, diversity schemes, and advanced propagation-aware radio network planning approaches.

Acknowledgments

This study was supported by the Ministry of Science, Technological Development and Innovation of the Republic of Serbia and these results are parts of the Grant No. 451-03-136/2025-03/200132 with University of Kragujevac – Faculty of Technical Sciences Cacak.

References

[1] PABST, R., WALKE, B. H., SCHULTZ, D. C., et al. Relay-based deployment concepts for wireless and mobile broadband radio. *IEEE Communications Magazine*, 2004, vol. 42, no. 9, p. 80–89. DOI: 10.1109/MCOM.2004.1336724

[2] SALEMA, C. *Microwave Radio Links: From Theory to Design*. Hoboken (NJ, USA): John Wiley & Sons, 2002. ISBN: 978-0-471-42026-2

[3] FREEMAN, R. L. *Radio System Design for Telecommunications*. 3rd ed. Hoboken (NJ, USA): John Wiley & Sons, 2007. ISBN: 978-0-470-05043-9

[4] GLIKSTEIN, O., PINHASI, G. A., PINHASI, Y. Scaled model for studying the propagation of radio waves diffracted from tunnels. *Electronics*, 2024, vol. 13, no. 10, p. 1–15. DOI: 10.3390/electronics13101983

[5] OHTA, S., NISHIO, T., KUDO, R., et al. Point cloud-based proactive link quality prediction for millimeter-wave communications. *IEEE Transactions on Machine Learning in Communications and Networking*, 2023, vol. 1, p. 258–276. DOI: 10.1109/TMLCN.2023.3319286

[6] MOYDUNOV, T., SARIMSAKOV, A., OMOROVA, S., et al. Analysis of radio relay station control system using IT-technologies. *Machinery & Energetics*, 2024, vol. 15, no. 4, p. 136–146. DOI: 10.31548/machinery/4.2024.136

[7] ABDULVASEA, M. O. A., ADYLBEKOVA, K. A. Methods for designing professional communication systems of TETRA standard, taking into account reliability indicators, *Synchroinfo Journal*, 2020, vol. 6, no. 6, p. 17–20. DOI: 10.36724/2664-066x-2020-6-6-17-20

[8] FERREIRA, E., SEBASTIÃO, C., CERCAS, F., et al. An optimized planning tool for microwave terrestrial and satellite link design. *Future Internet*, 2023, vol. 15, no. 2, p. 1–21. DOI: 10.3390/fi15020058

[9] ZHANG, X., ZHAO, Z., WU, Z., et al. Rain attenuation prediction model for terrestrial links incorporating wet antenna effects. *IET Microwaves, Antennas & Propagation*, 2023, vol. 17, no. 8, p. 634–641. DOI: 10.1049/mia2.12384

[10] SAMAD, M. A., DIBA, F. D., CHOI, D.-Y. A survey of rain attenuation prediction models for terrestrial links—current research challenges and state-of-the-art. *Sensors*, 2021, vol. 21, no. 4, p. 1–28. DOI: 10.3390/s21041207

[11] CHANDRA, D., YUSNITA, S., MEIDELFI, D., et al. Microwave link planning for USO/N3T telecommunication sites using Atoll radio planning software. *International Journal of Advanced Technology and Social Sciences*, 2025, vol. 3, no. 12, p. 1603 to 1616. DOI: 10.59890/ijatss.v3i12.150

[12] GAO, H., JIANG, T., LI, J., et al. Comparison of relay methods for long-distance radio frequency transmission. *Journal of Lightwave Technology*, 2024, vol. 42, no. 1, p. 121–127. DOI: 10.1109/JLT.2023.3304563

[13] VILA, I., SALLENT, O., PEREZ-ROMERO, J. Relay-empowered beyond 5G radio access networks with edge computing capabilities. *Computer Networks*, 2024, vol. 243, p. 1–11. DOI: 10.1016/j.comnet.2024.110287

[14] SUN, S., RAPPAPORT, T. S., SHAFI, M., et al. Propagation models and performance evaluation for 5G millimeter-wave bands, *IEEE Transactions on Vehicular Technology*, 2018, vol. 67, no. 9, p. 8422–8439. DOI: 10.1109/tvt.2018.2848208

[15] YANG, K., SHI, Z., QIN, L., et al. Performance evaluation of the radio propagation in a vessel cabin using LoRa bands. *Sensors*, 2025, vol. 26, no. 1, p. 1–18. DOI: 10.3390/s26010207

[16] UNGER, T. I., KUNCZMANN, M. The impact of terrain sampling density on 5G NR-V2X downlink channel modeling using various propagation models at the 3.6 GHz band. *Radioengineering*, 2025, vol. 34, no. 4, p. 603–623. DOI: 10.13164/re.2025.0603

[17] TATOVIC, A. Digital TETRA radio relay link design for the tunnel Laz–Ovčar section. In *Proceedings of the 25th International Symposium INFOTEH-JAHORINA*. Jahorina (Bosnia and Herzegovina), 2026, p. 1–4. DOI: 10.1109/INFOTEH68759.2026.11477675

[18] INTERNATIONAL TELECOMMUNICATION UNION. *Recommendation ITU-R F.636-5, Radio-Frequency Channel Arrangements for Fixed Wireless Systems Operating in the 14.4-15.35 GHz Band.* Nov. 2019.

[19] INTERNATIONAL TELECOMMUNICATION UNION. *Recommendation ITU-R P.1812-7, A Path-Specific Propagation Prediction Method for Point-to-Area Terrestrial Services in Frequency Range 30 MHz to 6 GHz.* Aug. 2023.

[20] INTERNATIONAL TELECOMMUNICATION UNION. *Recommendation ITU-R P.525-4, Calculation of Free-Space Attenuation.* Aug. 2019.

[21] INTERNATIONAL TELECOMMUNICATION UNION. *Recommendation ITU-R P.841-6, Conversion of Annual Statistics to Worst-Month Statistics.* Aug. 2019.

[22] INTERNATIONAL TELECOMMUNICATION UNION. *Recommendation* ITU-R P.453-13, *The Radio Refractive Index: Its Formula and Refractivity Data.* Aug. 2019.

[23] INTERNATIONAL TELECOMMUNICATION UNION. *Recommendation ITU-R P.837-7, Characteristics of Precipitation for Propagation Modelling.* Jun. 2017.

[24] INTERNATIONAL TELECOMMUNICATION UNION. *Recommendation ITU-R P.836-6, Water Vapour: Surface Density and Total Columnar Content.* Dec. 2017.

[25] INTERNATIONAL TELECOMMUNICATION UNION. *Recommendation ITU-R P.530-18, Prediction Methods Required for the Design of Terrestrial Line-Of-Sight Systems.* Sep. 2021.

[26] INTERNATIONAL TELECOMMUNICATION UNION. *Recommendation ITU-R P.526-15, Propagation by Diffraction.* Oct. 2019.

[27] INTERNATIONAL TELECOMMUNICATION UNION. *Recommendation* ITU-R P.676-13, *Attenuation by Atmospheric Gases and Related Effects*. Aug. 2022.

[28] INTERNATIONAL TELECOMMUNICATION UNION. *Recommendation* ITU-R P.678-3, *Characterization of the Variability of Propagation Phenomena and Estimation of the Risk Associated with Propagation Margin.* July 2015.

[29] INTERNATIONAL TELECOMMUNICATION UNION. *Recommendation ITU-R P.838-3, Specific Attenuation Model for Rain for Use in Prediction Methods*. Mar. 2005.

[30] INTERNATIONAL TELECOMMUNICATION UNION. *Recommendation ITU-R P.834-9, Effects of Tropospheric Refraction on Radiowave Propagation.* Dec. 2017.

[31] INTERNATIONAL TELECOMMUNICATION UNION. *Recommendation ITU-R P.840-8, Attenuation due to Clouds and Fog.* Aug. 2019.

[32] INTERNATIONAL TELECOMMUNICATION UNION. *Recommendation ITU-T G.821, Error Performance of an International Digital Connection Operating at a Bit Rate below the Primary Rate and Forming Part of an Integrated Services Digital Network*. Dec. 2002.

[33] INTERNATIONAL TELECOMMUNICATION UNION. *Recommendation ITU-R F.1668-1, Error Performance Objectives for Real Digital Fixed Wireless Links Used in 27 500 km Hypothetical Reference Paths and Connections*. 2007.

[34] INTERNATIONAL TELECOMMUNICATION UNION. *Recommendation ITU-R F.1703, Availability and Error Performance Objectives for Real Digital Fixed Wireless Links Used in 27 500 km Hypothetical Reference Paths and Connections.* 2005.

[35] OLSEN, R. L., TJELTA, T. Worldwide techniques for predicting the multipath fading distribution on terrestrial LOS links: Background and results of tests. *IEEE Transactions on Antennas and Propagation*, 1999, vol. 47, no. 1, p. 157–170. DOI: 10.1109/8.753006

[36] GOVERNMENT OF THE REPUBLIC OF SERBIA. Decree on the establishment of the radio frequency bands allocation plan, prepared by the Regulatory Authority for Electronic Communications and Postal Services (RATEL). *Official Gazette of the Republic of Serbia,* No. 76, August 29, 2025.

[37] ELECTRONIC COMMUNICATIONS COMMITTEE (ECC). The European Table of Frequency Allocations and Applications (ECA Table). *CEPT,* November 20, 2025.

[38] INTERNATIONAL TELECOMMUNICATION UNION. *Radio Regulations, Edition of 2024*. 2024.

[39] COUDÉ, R. *Radio Mobile: Radio propagation simulation software.* [Online]. Available: http://www.ve2dbe.com

About the Authors …

Ana TATOVIĆ (corresponding author) received the B.S. degree from the School of Electrical Engineering, University of Belgrade, Belgrade, Serbia, in 2008, and the M.Sc. degree from the same institution in 2013, and the Ph.D. degree from the Faculty of Technical Sciences in Čačak, University of Kragujevac, Serbia, in 2019. In 2013, she joined the Faculty of Technical Sciences in Čačak, University of Kragujevac, where she is currently an Assistant Professor. Her expertise includes RF/microwave filters, microwave passive circuits, electric circuit theory, and microwave engineering. Her research interests focus on the design and analysis of RF and microwave circuits and systems, as well as signal processing.

Marina MILOSEVIĆ received the Diploma degree in Electrical Engineering from the Faculty of Technical Sciences Čačak, University of Kragujevac, Čačak, Serbia, in 2010, and the Ph.D. degree in Electrical Engineering and Computing from the Faculty of Electronic Engineering, University of Niš, Niš, Serbia, in 2016. She is currently an Associate Professor with the Department of Computer and Software Engineering, Faculty of Technical Sciences Čačak, University of Kragujevac, Serbia. Her research interests include digital signal processing, image processing, biomedical engineering and medical informatics.

Đorđe DAMNJANOVIĆ received his B.Sc. degree in Computer Science in 2010 and M.Sc. degree in Computer Engineering in 2011, both from the Faculty of Technical Sciences Čačak, University of Kragujevac. He finished Ph.D. thesis at the Faculty of Electronic Engineering, University of Niš, Serbia, in 2022. Currently, he is an Assistant Professor at the Department of Computer and Software Engineering, Faculty of Technical Sciences Čačak, University of Kragujevac. His research interests include signal processing, image processing, remote control, and human-computer interaction.